Ability of dynamic gadoxetic acid–enhanced magnetic resonance imaging combined with water-specific T1 mapping to reflect inflammation in a rat model of early-stage nonalcoholic steatohepatitis

Qian Wan[1#], Hao Peng[1#], Feng Liu[2], Xiaoyi Liu[3], Chuanli Cheng[1], Changjun Tie[1], Jie Deng[4], Jianxun Lyu[5], Yizhen Jia[6], Yi Wang[3], Hairong Zheng[1], Dong Liang[1], Xin Liu[1], Chao Zou[1]

[1]Paul C. Lauterbur Research Center for Biomedical Imaging, Shenzhen Institute of Advanced Technology, Chinese Academy of Sciences, Shenzhen, China; [2]Peking University People's Hospital, Peking University Hepatology Institute, Beijing Key Laboratory of Hepatitis C and Immunotherapy for Liver Diseases, Beijing International Cooperation Base for Science and Technology on NAFLD Diagnosis, Beijing, China; [3]Departments of Radiology, Peking University People's Hospital, Beijing, China; [4]Department of Radiation Oncology, UT Southwestern Medical Center, Dallas, TX, USA; [5]Department of Radiology, The University of Hong Kong-Shenzhen Hospital, Shenzhen, China; [6]Departments of Research Services, The University of Hong Kong-Shenzhen Hospital, Shenzhen, China

Contributions: (I) Conception and design: Y Wang, J Deng; (II) Administrative support: C Zou; (III) Provision of study materials or patients: C Cheng; (IV) Collection and assembly of data: Q Wan, H Peng; (V) Data analysis and interpretation: F Liu, Xiaoyi Liu; (VI) Manuscript writing: All authors; (VII) Final approval of manuscript: All authors.

[#]These authors contributed equally to this work.

Correspondence to: Chao Zou, PhD. Paul C. Lauterbur Research Center for Biomedical Imaging, Shenzhen Institute of Advanced Technology, Chinese Academy of Sciences, No. 1068 Xueyuan Avenue, Nanshan District, Shenzhen 518055, China. Email: chao.zou@siat.ac.cn; Yi Wang, PhD, MD. Department of Radiology, Peking University People's Hospital, No. 11 Xizhimen South St, Beijing 100044, China. Email: wangyi@pkuph.edu.cn.

Background: Gadolinium ethoxybenzyl-diethylenetriaminepentaacetic acid (Gd-EOB-DTPA) has shown potential in reflecting the hepatic function alterations in nonalcoholic steatohepatitis (NASH). The purpose of this study was to evaluate whether Gd-EOB-DTPA combined with water-specific T1 (wT1) mapping can be used to detect liver inflammation in the early-stage of NASH in rats.

Methods: In this study, 54 rats with methionine- and choline-deficient (MCD) diet–induced NASH and 10 normal control rats were examined. A multiecho variable flip angle gradient echo (VFA-GRE) sequence was performed and repeated 40 times after the injection of Gd-EOB-DTPA. The wT1 of the liver and the reduction rate of wT1 (rrT1) were calculated. All rats were histologically evaluated and grouped according to the NASH Clinical Research Network scoring system. Quantitative real-time polymerase chain reaction (qRT-PCR) was performed to detect the expression of Gd-EOB-DTPA transport genes. Analysis of variance and least significant difference tests were used for multiple comparisons of quantitative results between all groups. Multiple regression analysis was applied to identify variables associated with precontrast wT1 (wT1$_{pre}$), and receiver operating characteristic (ROC) analysis was performed to assess the diagnostic performance.

Results: The rats were grouped according to inflammatory stage (G0 =4, G1 =15, G2 =12, G3 =23) and fibrosis stage (F0 =26, F1 =19, F2 =9). After the infusion of Gd-EOB-DTPA, the rrT1 showed significant differences between the control and NASH groups (P<0.05) but no difference between the different inflammation and fibrosis groups at any time points. The areas under curve (AUCs) of rrT1 at 10, 20, and 30 minutes were only 0.53, 0.58, and 0.61, respectively, for differentiating between low inflammation grade (G0 + G1) and high inflammation grade (G2 + G3). The MRI findings were verified by qRT-PCR examination, in which the Gd-EOB-DTPA transporter expressions showed no significant differences

between any inflammation groups.

Conclusions: The wT1 mapping quantitative method combined with Gd-EOB-DTPA was not capable of discerning the inflammation grade in a rat model of early-stage NASH.

Keywords: Magnetic resonance imaging (MRI); water-specific T1 (wT1) mapping; gadolinium ethoxybenzyl-diethylenetriaminepentaacetic acid (Gd-EOB-DTPA); nonalcoholic steatohepatitis (NASH)

Introduction

Nonalcoholic fatty liver disease (NAFLD), which ranges in severity from simple steatosis to a more serious subtype of nonalcoholic steatohepatitis (NASH), is now the leading cause of chronic liver disease (1). NASH is histologically diagnosed via the severity of steatosis, hepatocyte ballooning, and inflammation from liver biopsy (2). In the majority of individuals, NASH is symptomless and may progress silently toward cirrhosis or even hepatocellular carcinoma (3). Therefore, the noninvasive assessment of disease severity is critical to preventing disease progression in patients with NASH (4). Recently, several magnetic resonance imaging (MRI) methods such as MR elastography (MRE) and the quantitative T1 mapping-based MRI have demonstrated promising results in identifying high-risk NASH through examining liver stiffness or extracellular volume fraction (5-8).

Gadolinium ethoxybenzyl-diethylenetriaminepentaacetic acid (Gd-EOB-DTPA), a hepatocyte-specific contrast agent, can be used to detect liver lesions or evaluate hepatic functions (9-11). Gd-EOB-DTPA can be specifically taken up by the hepatocytes through organic anion-transporting polypeptide transporters (OATPs) located on the sinusoidal hepatocellular membrane and excreted into the biliary system via multidrug resistance protein 2 (MRP2) located on the canalicular hepatocellular membrane (12). The expression of these transporters can be affected by NASH (13). Several studies have reported that Gd-EOB-DTPA uptake in the T1 change of liver can be used to differentiate NASH from the simple steatosis or to stage advanced fibrosis in NAFLD (14,15). In most of the studies examining Gd-EOB-DTPA, quantitation was completed via relative liver enhancement (RLE) as calculated from the signal intensity (SI) of the T1-weighted images (13,16,17). However, the SI in T1-weighted images can be confounded by a variety of factors, such as imaging parameters, field inhomogeneity,

and the receiver coil sensitivity (18); moreover, a recent study revealed that the T1 value is highly correlated with the level of hepatic steatosis (19). On the other hand, T1 relaxation time mapping provides more reliable tissue characterization and can evaluate the hepatic function quantitatively by revealing the relative T1 change induced by Gd-EOB-DTPA administration (18). However, it should be noted that T1 mapping in NAFLD may also be confounded by intracellular hepatocyte lipids (20). In our previous study, water-specific T1 (wT1) mapping could address the interference of liver steatosis if the T1 was calculated solely depending on the water component of the liver. The ability of wT1 to assess the levels of liver inflammatory activity was validated in a methionine- and choline-deficient (MCD) diet-induced NAFLD rat model (21).

Therefore, the aim of this study was to evaluate whether the wT1 mapping method combined with Gd-EOB-DTPA administration is able to characterize the severity of inflammation in the early stage of NASH, defined as fibrosis stage (F) ≤2 (22), in an MCD diet rat model.

Methods

Animal model

This study was performed under a project license (no. SIAT-IACUC-210901-YGS-LX-A2045) granted by the Institutional Animal Care Committee at the Shenzhen Institute of Advanced Technology, in compliance with institutional guidelines for the care and use of animals. A total of 65 male Wistar rats that were approximately 4 weeks old were obtained from Beijing Vital River Laboratory Animal Technology Co., Ltd. The rats were divided into two groups: a control group (n=10) fed with a standard chow ad libitum and a NASH group (n=55) fed with the MCD diet (A02082002BR; Research Diets Inc.) for 2, 4, 5, 6, and 8 weeks, respectively. Ultimately, 64 rats

were included in the study (10 controls and 54 MCD rats), and the remaining 1 rat was excluded due to poor image quality with evident motion artifacts.

Pathological assessment

All animals were humanely euthanized with pentobarbital sodium (150 mg/kg) after MR examination. The livers were rapidly exteriorized, and the left lobes of the liver were embedded and fixed in 10% formalin for paraffin section. Liver sections were stained with hematoxylin and eosin (HE) and Sirius red to observe the hepatic pathologic structure and liver fibrosis. The severity of histological changes was assessed by a liver pathologist (F.L., with 20 years of working experience). The liver pathological score was evaluated according to the NASH Clinical Research Network (CRN) histological scoring system via the following ordinal scales: steatosis was graded according to the percentage of hepatocytes that contained fat (S0 for less than 5%, S1 for 5–33%, S2 for 33–66%, and S3 for more than 66%); lobular inflammation grade was scored as G0 (none), G1 (mild: <2 foci per 200 × field), G2 (moderate: 2–4 foci per 200 × field), or G3 (severe: >4 foci per 200 × field); and fibrosis grade was evaluated as F0 (none), F1 (perisinusoidal or periportal fibrosis), or F2 (perisinusoidal and periportal fibrosis) (23).

Image acquisition

The animals were anesthetized with isoflurane and underwent MRI examination on a 3.0 T clinical MR scanner (uMR790; Shanghai United Imaging Healthcare, Shanghai, China) with a 12-channel small animal coil. The abdomen was secured with a belt to decrease respiratory motion artifacts. A multiecho variable flip angle GRE (VFA-GRE) sequence was performed before and after the injection of 0.125 mmol/kg of Gd-EOB-DTPA (Primovist; Bayer Schering Pharma, Berlin, Germany) manually administered via the tail vein. The parameters of the VFA-GRE were as follows: TR =20.5 ms, TE =3.45/4.92/6.39/7.86/9.33/10.8 ms, 1 slice acquired using a 2.0-mm slice thickness, field of view =80 mm × 60 mm, image matrix =128×96, flip angle =3°/7°/11°/15°, number of average for data acquisition =10, and parallel imaging with an acceleration rate of 2. The acquisition time of VFA-GRE was 1 minute for each scan. The VFA-GRE sequence was continuously repeated 40 times after Gd-EOB-DTPA administration. A dual refocusing echo acquisition mode (DREAM) B1+ mapping sequence was applied to correct B1

heterogeneity with the following parameters: TR =6.9 ms, TE =2.24 ms, 1 slice acquired using a 5.0-mm slice thickness, field of view =96 mm ×65 mm, image matrix =48×33, and acquisition time =0.2 s.

Image analysis

The proton density fat fraction (PDFF) and water-only images were first obtained through the fat–water separation algorithm proposed in a previous study using the multiecho images under each flip angle (20). Briefly, the 6-peak fat spectral model was used to quantify the PDFF from the separated fat and water signals under a flip angle of 3°. The wT1 mapping of the liver was then fitted from these water-only images under varying flip angles corrected by the B1+ mapping.

The wT1 was estimated according to the following equation (21):

$$W_\theta = M_w \frac{1 - e^{-TR/wT_1}}{1 - e^{-TR/wT_1} \cdot \cos(b_1\theta)} \cdot \sin(b_1\theta) \qquad [1]$$

where W_θ is the SI of the water component under the corresponding flip angle, θ is the nominal flip angle set in the imaging sequence, Mw is the indicator of the net magnetization at equilibrium of water protons, and b1 is the relative radio frequency (RF) emission field (B1+) inhomogeneity.

All MR images were evaluated by two radiologists (H.P. and J.L.) who were supervised by a radiologist (Y.W.) with 20 years' experience. Three regions of interest (ROIs) of the same pixel number were placed on the wT1 images containing most liver parenchyma before and after Gd-EOB-DTPA enhancement, with the inclusion of blood vessels and bile ducts being avoided; refer to a previous study for details (21). The wT1 values at each time point were averaged over the pixels from all three ROIs. The rrT1 at each time point after the Gd-EOB-DTPA enhancement was defined as follows:

$$rrT1(\%) = \left[\left(T1_{pre} - T1_{post} \right) / T1_{pre} \right] \times 100 \qquad [2]$$

where $T1_{pre}$ and $T1_{post}$ are the wT1 relaxation times of the pre– and post–Gd-EOB-DTPA injection, respectively.

Quantitative real-time polymerase chain reaction analysis

To further verify whether the Gd-EOB-DTPA transporters are correlated with disease severity, we compared the

uptake transporters of oraginc anion transporting polypeptides (Oatp1a1 and Oatp1b2) and Na$^+$-taurocholate co-transporting polypeptide (Ntcp) and the excretion transporters of Mrp2 mRNA expression using quantitative real-time polymerase chain reaction (qRT-PCR) examinations.

Liver samples were collected and frozen at –80 ℃ for qRT-PCR examination. Total RNA was extracted with TRIzol reagent (Invitrogen, Thermo Fisher Scientific, Waltham, MA, USA) and was subsequently subjected to reverse transcription to generate complement DNA (cDNA) with a PrimeScript RT reagent kit (Takara Bio, Tokyo, Japan). The expression of target genes was determined using TB Green Premix Ex Taq (Takara Bio). Specific primer sets (forward and reverse) for genes of Oatp1a1, Oatp1b2, Ntcp, and Mrp2 were as follows: Oatp1a1, 5'-CTGGTATTCCCGCACCTGTTT-3' and 5'-CTGTGTGCTCGCTTTCCTTCTC-3'; Oatp1b2, 5'-CCTGTTCAAGTTCATAGAGCAGCA-3' and 5'-TGCCATAGTAGGTATGGTTATAATTCCTAA-3'; Ntcp, 5'-CTCACTTGTGGAAGCCCAAAG-3' and 5'-TCACGATGCTGAGGTTCATGTC-3'; and Mrp2, 5'-ATCGCTCACAGGCTGCACAC-3' and 5'-TCAGGACTGCCATACTCGACAATC-3'. The relative expression levels were normalized to the housekeeping gene glyceraldehyde phosphate dehydrogenase (Gapdh) with a forward primer of 5'-GGCACAGTCAAGGCTGAGAATG-3' and a reverse primer of 5'-ATGGTGGTGAAGACGCCAGTA-3'. PCR amplification was performed using the Thermal Cycler Dice TP800 (Takara Bio) and a SYBR Premix Ex Taq II Kit (Perfect Real Time; Takara Bio) after reverse transcription.

Statistical analysis

All statistical analyses were performed with SPSS version 25.0 (IBM Corp.). Data are presented as mean ± standard deviation (SD). The analysis of variance followed by the least significant difference (LSD) for multiple comparisons were used to compare the quantitative results between different levels of inflammation and fibrosis. Multiple linear regression with stepwise selection was used to identify histopathologic parameters (inflammation and fibrosis) that independently correlated with precontrast wT1 (wT1$_{pre}$). The diagnostic performance of rrT1 in the assessment of liver inflammation was evaluated by calculating the receiver operating characteristic curve (AUROC) via ROC analysis. The accuracy, sensitivity, and specificity for detecting the grade of inflammation were determined using the thresholds for maximizing the Youden index, and 95% confidence intervals (CIs) were estimated in the ROC analysis. A P value <0.05 was considered statistically significant in all tests.

Results

Histology of the experimental model

In the histopathologic findings from the HE and Sirius-red staining, as shown in *Figure 1*, diffuse macrovesicular steatosis, lobular inflammation, and perisinusoidal and/or periportal fibrosis were observed in the NASH group, whereas these features were not found in the control group. According to the scoring system proposed by NASH-CRN (23), the rats in NASH group were categorized in terms of steatohepatitis (S3 =54, all rats), lobular inflammation grade (G0 =4, G1 =15, G2 =12, G3 =23), and fibrosis stage (F0 =26, F1 =19, F2 =9). G0 + G1 and G2 + G3 were combined into a none-to-mild inflammation group (GL; n=19) and a moderate-to-severe grade group (GH; n=35), respectively; F0 was defined as the no-fibrosis group (n=26), and F1 + F2 were combined into a mild-to-moderate fibrosis group (FL; n=28).

MRI measurements

The PDFF of NASH rats with inflammation of GL (27.60 ± 6.32%) was similar to that of GH rats (30.00%±8.30%) (P>0.05) and was significantly higher than that of the control rats (5.95%±0.47%) (P<0.05).

Typical wT1 images obtained precontrast (wT1$_{pre}$) and 10, 20, and 30 minutes after Gd-EOB-DTPA administration in the control and NASH groups are shown in *Figure 2*. The wT1$_{pre}$ values in the different inflammation or fibrosis groups were as follows: control 512.76±76.42 ms, GL 578.81±63.77 ms, GH 516.20±63.03 ms, F0 553.16±84.71 ms, and FL 524.37±49.43 ms. The wT1$_{pre}$ of the GL group was significantly higher than that of the GH group (P<0.05). However, there was no significant difference between the fibrosis groups (F0 *vs.* FL) (*Table 1*).

After the infusion of Gd-EOB-DTPA, the dynamic wT1 change profiles were observed across different inflammation grades (Figure S1A), and there were significant differences between the GL and GH groups at some time point. However, this difference may be determined by the wT1$_{pre}$ measured from the native liver before Gd-EOB-
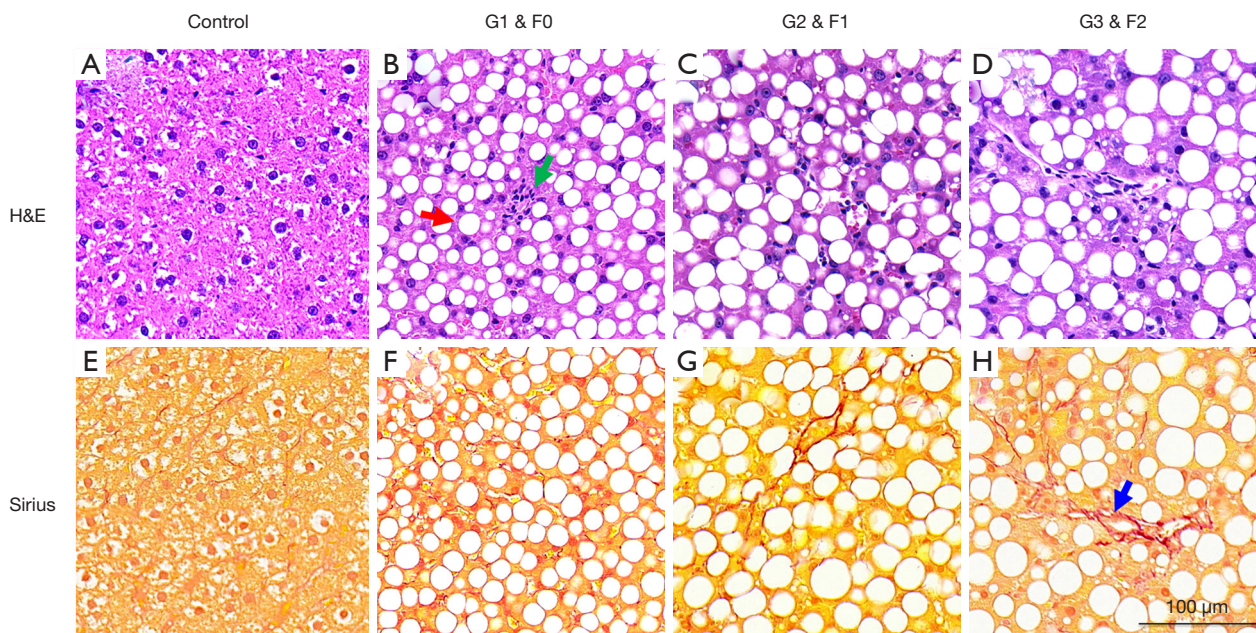
Figure 1 Representative liver histological sections from the control and NASH groups stained with hematoxylin and eosin (top) and Sirius red (bottom) (×200). Diffuse steatosis (S3, red arrow), inflammatory (G0–G3, green arrow), and fibrosis (F1–F2, blue arrow) infiltration were observed in the NASH group. Scale bar =100 µm. G1, mild inflammation; G2, moderate inflammation; G3, severe inflammation; F0, no fibrosis; F1, mild fibrosis; F2, moderate fibrosis; NASH, nonalcoholic steatohepatitis; H&E, hematoxylin and eosin.

DTPA administration (Figure S1B). Therefore, rrT1 was considered as being more appropriate for the quantitative assessment of Gd-EOB-DTPA uptake. The rrT1 values classified according to inflammation and fibrosis grades are shown in *Figure 3*. The rrT1 of the control group showed a gradual increase and peaked at 10 minutes. Meanwhile, the rrT1 in the hepatic inflammation and fibrosis groups immediately approached a maximum and then gradually declined. The rrT1 almost entirely overlapped between GL and GH groups or between F0 and F1 groups, and showed no significant difference (P>0.05). The representative rrT1 values at several time points are provided in *Table 1*. Furthermore, the rrT1 results according to the feed times of rats at 2, 4, 5, 6, and 8 weeks also showed no significant difference (Figure S2).

To further analyze the effect of fibrosis on the wT1 changes, we analyzed the $wT1_{pre}$ values in the no-fibrosis group (F0 =26 rats) and the GH group (GH =35 rats). As shown in Figure S3, the $wT1_{pre}$ of the GL group (n=19) with F0 was higher than that of the GH group (n=7) (P<0.05), but there was no significant difference in $wT1_{pre}$ between any grades of fibrosis in the GH inflammation group (P>0.05). Multivariate analysis showed that the inflammation stage was the main factor that independently influenced $wT1_{pre}$ in this study, explaining 17.0% of the variance in its value (R^2=0.17; β=–0.506; P<0.01), as shown in Table S1. However, liver fibrosis was not the dominant factor contributing to $wT1_{pre}$.

ROC analysis

Figure 4 shows the ROC curves of rrT1 at 10 minutes (rrT1-10 min), rrT1 at 20 minutes (rrT1-20 min), and rrT1 at 30 minutes (rrT1-30 min) for the differentiation between the GL group and GH group according to AUROCs. The results showed that rrT1-20 min has a somewhat higher performance (AUROC = 0.61; 95% CI: 0.45–0.76) than did rrT1-10 min (AUROC =0.58; 95% CI: 0.43–0.74) and rrT1-30 min (AUROC =0.53; 95% CI: 0.37–0.69). The cutoff value of rrT1-20 min was 44.34 %, with a sensitivity of 84.2% and a specificity of 40.0%.

qRT-PCR analysis

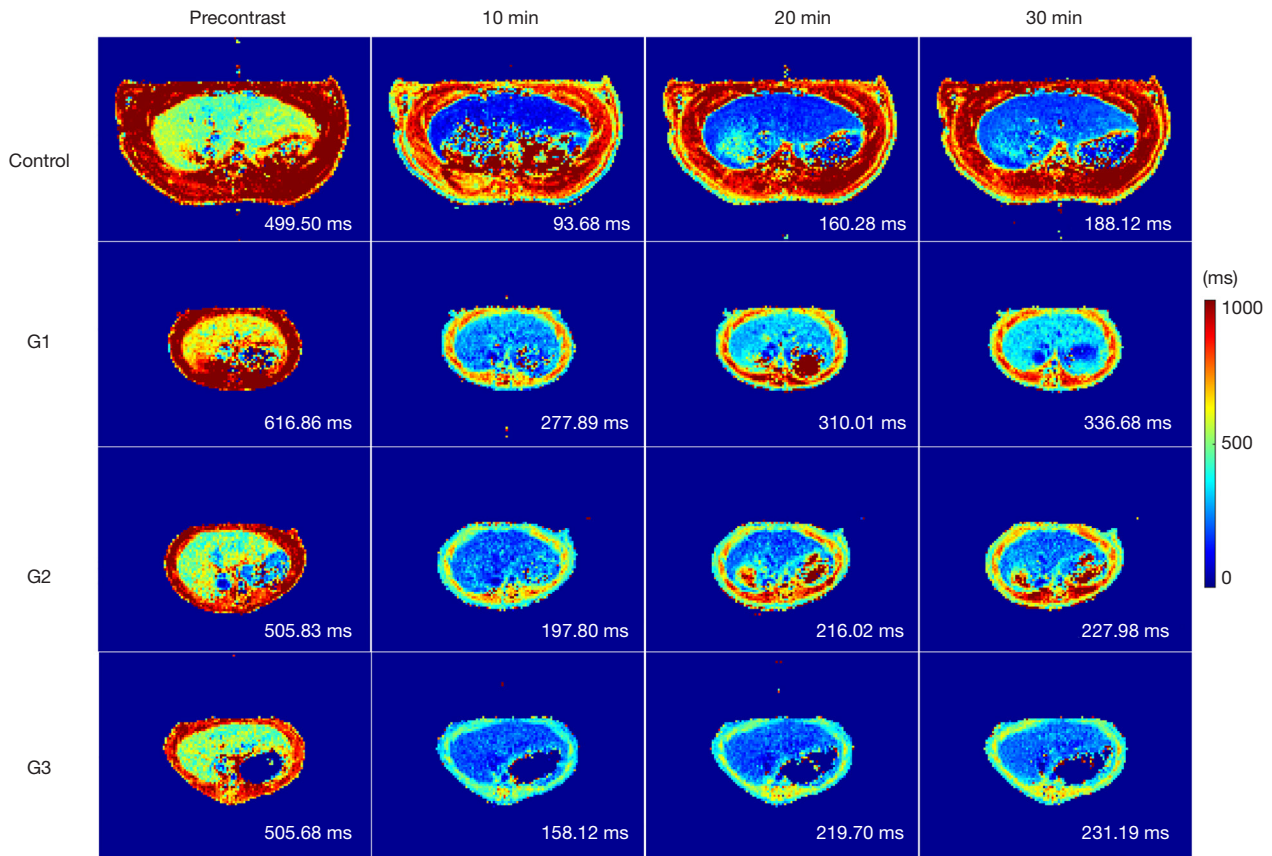The uptake and excretion of Gd-EOB-DTPA are mediated by the specific transmembrane transporters on

Figure 2 Typical wT1 images of Gd-EOB-DTPA–enhanced MRI in the control group (upper) and NASH group (lower) at several different time points (precontrast and 10, 20, and 30 minutes after Gd-EOB-DTPA administration). G1, mild inflammation; G2, moderate inflammation; G3, severe inflammation; NASH, nonalcoholic steatohepatitis; MRI, magnetic resonance imaging; wT1, water-specific T1; Gd-EOB-DTPA, gadolinium ethoxybenzyl-diethylenetriaminepentaacetic acid.

Table 1 The $wT1_{pre}$ and rrT1 (%) in the control and NASH groups classified according to the different levels of inflammation and fibrosis grade

Group	Precontrast	Postcontrast (rrT1)				
		5 min	10 min	20 min	30 min	40 min
Control	512.76±76.42	73.91±5.04	74.15±7.06	67.83±3.91	54.92±3.82	44.36±5.92
Inflammation						
GL	578.81±63.77	61.23±7.07	57.48±8.05	52.99±8.99	45.08±9.02	39.74±9.21
GH	516.20±63.03	60.48±9.52	59.97±9.22	49.48±10.81	46.38±11.90	41.25±10.67
Fibrosis						
F0	553.16±84.71	61.79±9.13	59.71±9.32	51.36±10.48	44.73±10.36	39.22±10.36
FL	524.37±49.43	59.77±8.27	58.52±8.49	50.12±10.21	47.03±11.46	42.11±9.87

Gd-EOB-DTPA, gadolinium ethoxybenzyl-diethylenetriaminepentaacetic acid; wT1, water-specific T1; rrT1, reduction rate of water-specific T1 after Gd-EOB-DTPA enhancement; GL, none-to-mild inflammation group (G0 + G1); GH, moderate-to-severe inflammation group (G2 + G3); F0, no-fibrosis group; FL, mild-to-moderate fibrosis group (F1 + F2).
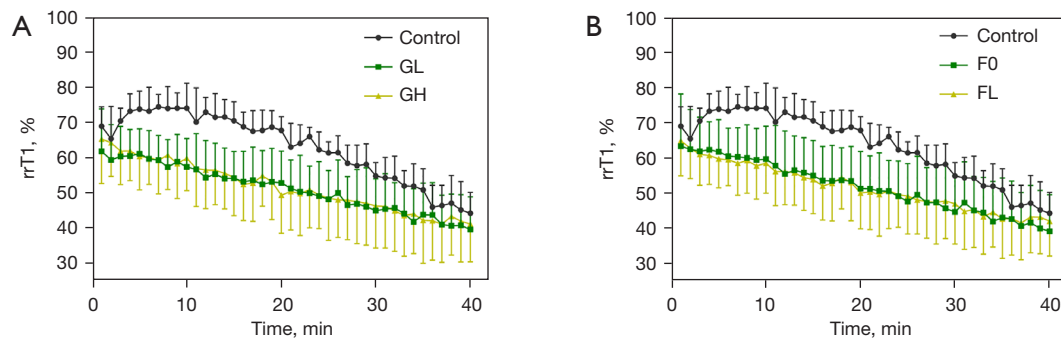
Figure 3 The dynamic rrT1 change profiles after Gd-EOB-DTPA administration across various inflammation grades (A) and fibrosis grades (B). Gd-EOB-DTPA, gadolinium ethoxybenzyl-diethylenetriaminepentaacetic acid; rrT1, reduction rate of water-specific T1 after Gd-EOB-DTPA enhancement; GL, none-to-mild inflammation group (G0 + G1); GH, moderate-to-severe inflammation group (G2 + G3); F0, no-fibrosis group; FL, mild-to-moderate fibrosis group (F1 + F2).
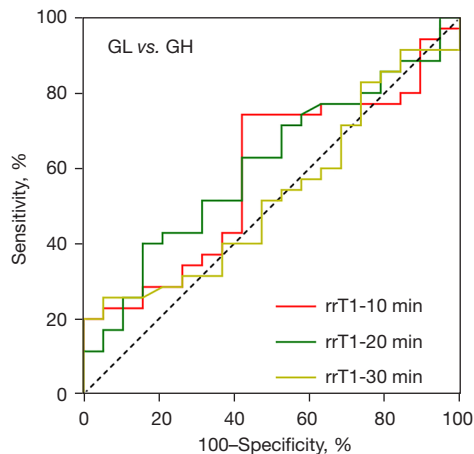
Figure 4 The ROC curves of rrT1-10 min, rrT1-20 min, and rrT1-30 min for dichotomized groups according to inflammation grade. Gd-EOB-DTPA, gadolinium ethoxybenzyl-diethylenetriaminepentaacetic acid; wT1, water-specific T1; rrT1, reduction rate of water-specific T1 after Gd-EOB-DTPA enhancement; GL, none-to-mild inflammation group (G0 + G1); GH, moderate-to-severe inflammation group (G2 + G3).

hepatocytes. To further verify whether the Gd-EOB-DTPA transporters change with the disease severity, we compared the expression of uptake transporters (Oatp1a1, Oatp1b2, Ntcp) and the excretion transporter Mrp2 using qRT-PCR. As shown in *Figure 5*, the expressions of Oatp1a1, Oatp1b2, Ntcp, and Mrp2 in NASH were significantly decreased compared to those of the control group (P<0.05). However, there was almost no significant difference observed between any of the inflammation or fibrosis stage groups.

Discussion

In this study, we aimed to evaluate the feasibility of Gd-EOB-DTPA with the wT1 technique for the noninvasive assessment of early-stage NASH in MCD diet–induced NASH in rats. The principal results indicated that the administration of Gd-EOB-DTPA combined with the wT1 quantitative method was not helpful in determining the inflammation severity in early-stage NASH rats.

The intracellular hepatocyte lipid has been demonstrated to be a strong confounding factor in T1 quantitative results for patients with NAFLD (19). Therefore, we used the wT1 mapping to measure the changes of Gd-EOB-DTPA to eliminate the interference of liver steatosis by calculating T1 only on the water component using the fat–water separation algorithm (20,21). The accuracy of the wT1 measurement has been validated by MR spectroscopy phantom experiments (21).

In our previous report, we found that the $wT1_{pre}$ of mild inflammation (G1) was higher than that of the other groups and that $wT1_{pre}$ could be used to differentiate between moderate-to-severe grade (G2 + G3) inflammation and none-to-mild grade (G0 + G1) inflammation, with an AUROC of 0.79 and a high sensitivity and specificity of 90% and 76%, respectively (21). The elevated $wT1_{pre}$ value in the mild-inflammation grade rats as compared with controls may be attributed to the increased free fluid in the hepatic extracellular matrix in the early stages of inflammation, when the inflammatory cells infiltrate the hepatic interstitial space and the vascular endothelial cell space expands, leading to fluid extravasation and cell edema (7,24). The reduction in $wT1_{pre}$ values with higher levels
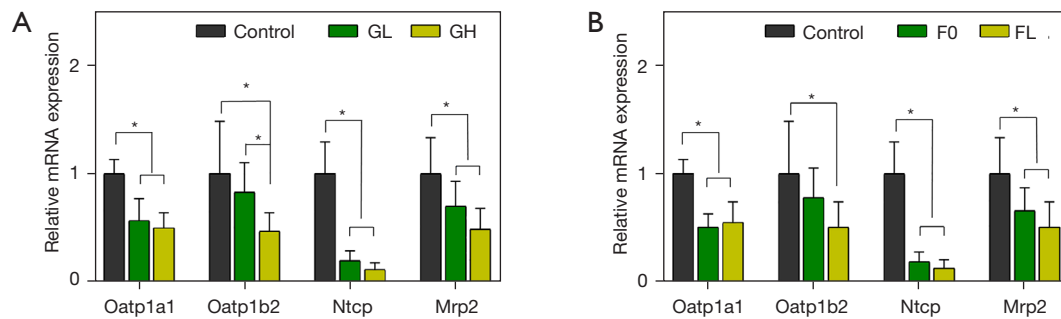
1598

Wan et al. Gd-EOB-DTPA with wT1 to reflect early-stage NASH

Figure 5 The comparison of Oatp1a1, Oatp1b2, Ntcp, and Mrp2 expression in each group across various inflammation grades (A) and fibrosis grades (B). *, P<0.05. mRNA, messenger RNA; GL, none-to-mild inflammation group (G0 + G1); GH, moderate-to-severe inflammation group (G2 + G3); F0, no-fibrosis group; FL, mild-to-moderate fibrosis group (F1 + F2).

of inflammation may be attributed to hepatocyte necrosis or changes in inflammation and cellular swelling (21). Moreover, it should be noted that fibrosis may also be an important factor in the wT1 change in NASH. However, according to our analysis, non-advanced fibrosis (F0–F2) had a relatively small effect on the wT1 results, which is consistent with previous reports (25).

We hypothesized that the hepatocyte-specific contrast of Gd-EOB-DTPA combined with wT1 mapping has the potential to more accurately reflect the inflammation and fibrosis stage in NASH progression than can a method based on wT1 alone (26). After administration of Gd-EOB-DTPA, we found that rrT1 was almost significantly lower in the inflammation and fibrosis group of the NASH rats than in the control rats, which is consistent with previous research (18). It is well known that the relative level of transmembrane transporters of OATPs and MRPs are the key determinants of hepatocellular uptake and excretion of Gd-EOB-DTPA molecules (13). In the qRT-PCR analysis, the expression of OATPs and MRPs genes in the NASH group were significantly decreased compared to that of the control group, which could have resulted in the decrease of Gd-EOB-DTPA accumulation in the NASH group (27).

However, the rrT1 results showed no significant differences between rats with different feeding periods. Moreover, no significant difference was found in the rrT1 between any of the inflammation or fibrosis groups at any time after Gd-EOB-DTPA injection. The possible reason for this may be that the expression of OATPs or MRPs was similar between the inflammation and fibrosis groups in our study. In a previous study, no significant correlation was found between Oatp1 expression and fibrosis stage, but there was a negative correlation between fibrosis stage and

Mrp2 expression in NASH (13). Therefore, we believe that our study is only valid for the early stage of NASH, and the results would be different if the advanced-stage NASH models were used.

Another previous study reported that the precontrast T1 and rrT1 at the hepatobiliary phase with Gd-EOB-DTPA were significantly different between a no-fibrosis (F0) group and significant-fibrosis (F2) group in a rabbit NAFLD model, which is not in line with our findings (18). This can be largely attributed to the different T1 quantification methods used. The possible interference in T1 mapping caused by the presence of fat was not fully considered in previous studies (25,28). Recent research has shown that intracellular hepatocyte lipid is a strong confounder for T1 quantification in patients with NAFLD (19,29), and it has even been demonstrated that severe liver steatosis (>30%) may confound detection performed according to distribution of Gd-EOB-DTPA (30). However, the wT1 mapping technique used in our previous phantom study showed good accuracy and independence from the fat fraction (20). Another possible reason for these discrepancies might be that we used the early stage of an animal NASH model (F ≤2), in which the OATP or MRP genes responsible for the transport of Gd-EOB-DTPA were not yet significantly altered.

There were some limitations to our study that should be mentioned. First, some of groups included were relatively small. For example, all the model rats had a steatosis level of S3, and there were only four rats with G0. The limit of the MCD-diet–induced NASH model prevented a more detailed analysis between simple steatosis and NASH. Second, due to the absence of more advanced hepatic fibrosis and cirrhosis (F3 + F4) in our rat NASH model,

the findings may not accurately reveal the various stages of the NAFLD. Third, the MCD-diet–induced NASH model that we used differs in terms of the pathological changes of human NAFLD; for example, hepatocellular ballooning is not prominent in the rat model (31). Finally, we did not compare our method with other indices or MRI approaches, such as hepatocyte uptake ratio and Gd-EOB-DTPA–enhanced T1ρ imaging (32).

Conclusions

Our finding indicates that use of Gd-EOB-DTPA combined with the wT1 quantitative method is unable to characterize the inflammation grade in a rat model of early-stage NASH.

Acknowledgments

Footnote

Conflicts of Interest: All authors have completed the ICMJE uniform disclosure form (available at https://qims.amegroups.com/article/view/10.21037/qims-23-482/coif). D.L. serves as an unpaid editorial board member of *Quantitative Imaging in Medicine and Surgery*. The other authors have no conflicts of interest to declare.

Ethical Statement: The authors are accountable for all aspects of the work in ensuring that questions related to the accuracy or integrity of any part of the work are appropriately investigated and resolved. The animals examined in this study under a project license (No. SIAT-IACUC-210901-YGS-LX-A2045) granted by the Institutional Animal Care Committee at the Shenzhen Institute of Advanced Technology, in compliance with institutional guidelines for the care and use of animals.

Open Access Statement: This is an Open Access article distributed in accordance with the Creative Commons Attribution-NonCommercial-NoDerivs 4.0 International License (CC BY-NC-ND 4.0), which permits the non-commercial replication and distribution of the article with the strict proviso that no changes or edits are made and the original work is properly cited (including links to both the formal publication through the relevant DOI and the license). See: https://creativecommons.org/licenses/by-nc-nd/4.0/.

References

1. Sheka AC, Adeyi O, Thompson J, Hameed B, Crawford PA, Ikramuddin S. Nonalcoholic Steatohepatitis: A Review. JAMA 2020;323:1175-83.
2. Loomba R, Friedman SL, Shulman GI. Mechanisms and disease consequences of nonalcoholic fatty liver disease. Cell 2021;184:2537-64.
3. Powell EE, Wong VW, Rinella M. Non-alcoholic fatty liver disease. Lancet 2021;397:2212-24.
4. Eslam M, Newsome PN, Sarin SK, Anstee QM, Targher G, Romero-Gomez M, et al. A new definition for metabolic dysfunction-associated fatty liver disease: An international expert consensus statement. J Hepatol 2020;73:202-9.
5. Tang A, Dzyubak B, Yin M, Schlein A, Henderson WC, Hooker JC, Delgado TI, Middleton MS, Zheng L, Wolfson T, Gamst A, Loomba R, Ehman RL, Sirlin CB. MR elastography in nonalcoholic fatty liver disease: inter-center and inter-analysis-method measurement reproducibility and accuracy at 3T. Eur Radiol 2022;32:2937-48.
6. Pavlides M, Banerjee R, Tunnicliffe EM, Kelly C, Collier J, Wang LM, Fleming KA, Cobbold JF, Robson MD, Neubauer S, Barnes E. Multiparametric magnetic resonance imaging for the assessment of non-alcoholic fatty liver disease severity. Liver Int 2017;37:1065-73.
7. Luetkens JA, Klein S, Träber F, Schmeel FC, Sprinkart AM, Kuetting DLR, Block W, Uschner FE, Schierwagen R, Hittatiya K, Kristiansen G, Gieseke J, Schild HH, Trebicka J, Kukuk GM. Quantification of Liver Fibrosis at T1 and T2 Mapping with Extracellular Volume Fraction MRI: Preclinical Results. Radiology 2018;288:748-54.
8. Schaapman JJ, Tushuizen ME, Coenraad MJ, Lamb HJ. Multiparametric MRI in Patients With Nonalcoholic Fatty Liver Disease. J Magn Reson Imaging 2021;53:1623-31.
9. Haimerl M, Fuhrmann I, Poelsterl S, Fellner C, Nickel MD, Weigand K, Dahlke MH, Verloh N, Stroszczynski C, Wiggermann P. Gd-EOB-DTPA-enhanced T1 relaxometry for assessment of liver function determined

by real-time (13)C-methacetin breath test. Eur Radiol 2018;28:3591-600.

10. Watanabe H, Kanematsu M, Goshima S, Kondo H, Onozuka M, Moriyama N, Bae KT. Staging hepatic fibrosis: comparison of gadoxetate disodium-enhanced and diffusion-weighted MR imaging--preliminary observations. Radiology 2011;259:142-50.

11. Kim JE, Kim HO, Bae K, Choi DS, Nickel D. T1 mapping for liver function evaluation in gadoxetic acid-enhanced MR imaging: comparison of look-locker inversion recovery and B(1) inhomogeneity-corrected variable flip angle method. Eur Radiol 2019;29:3584-94.

12. Choi Y, Huh J, Woo DC, Kim KW. Use of gadoxetate disodium for functional MRI based on its unique molecular mechanism. Br J Radiol 2016;89:20150666.

13. Tsuda N, Matsui O. Signal profile on Gd-EOB-DTPA-enhanced MR imaging in non-alcoholic steatohepatitis and liver cirrhosis induced in rats: correlation with transporter expression. Eur Radiol 2011;21:2542-50.

14. Bastati N, Feier D, Wibmer A, Traussnigg S, Balassy C, Tamandl D, Einspieler H, Wrba F, Trauner M, Herold C, Ba-Ssalamah A. Noninvasive differentiation of simple steatosis and steatohepatitis by using gadoxetic acid-enhanced MR imaging in patients with nonalcoholic fatty liver disease: a proof-of-concept study. Radiology 2014;271:739-47.

15. Hayashi T, Saitoh S, Fukuzawa K, Tsuji Y, Takahashi J, Kawamura Y, Akuta N, Kobayashi M, Ikeda K, Fujii T, Miyati T, Kumada H. Noninvasive Assessment of Advanced Fibrosis Based on Hepatic Volume in Patients with Nonalcoholic Fatty Liver Disease. Gut Liver 2017;11:674-83.

16. Wu Z, Matsui O, Kitao A, Kozaka K, Koda W, Kobayashi S, Ryu Y, Minami T, Sanada J, Gabata T. Usefulness of Gd-EOB-DTPA-enhanced MR imaging in the evaluation of simple steatosis and nonalcoholic steatohepatitis. J Magn Reson Imaging 2013;37:1137-43.

17. Yamada T, Obata A, Kashiwagi Y, Rokugawa T, Matsushima S, Hamada T, Watabe H, Abe K. Gd-EOB-DTPA-enhanced-MR imaging in the inflammation stage of nonalcoholic steatohepatitis (NASH) in mice. Magn Reson Imaging 2016;34:724-9.

18. Ding Y, Rao SX, Meng T, Chen C, Li R, Zeng MS. Usefulness of T1 mapping on Gd-EOB-DTPA-enhanced MR imaging in assessment of non-alcoholic fatty liver disease. Eur Radiol 2014;24:959-66.

19. Ahn JH, Yu JS, Park KS, Kang SH, Huh JH, Chang JS, Lee JH, Kim MY, Nickel MD, Kannengiesser S, Kim JY,

Koh SB. Effect of hepatic steatosis on native T1 mapping of 3T magnetic resonance imaging in the assessment of T1 values for patients with non-alcoholic fatty liver disease. Magn Reson Imaging 2021;80:1-8.

20. Peng H, Cheng C, Wan Q, Jia S, Wang S, Lv J, Liang D, Liu W, Liu X, Zheng H, Zou C. Fast multi-parametric imaging in abdomen by B1+ corrected dual-flip angle sequence with interleaved echo acquisition. Magn Reson Med 2022;87:2194-208.

21. Wan Q, Peng H, Lyu J, Liu F, Cheng C, Qiao Y, Deng J, Zheng H, Wang Y, Zou C, Liu X. Water Specific MRI T1 Mapping for Evaluating Liver Inflammation Activity Grades in Rats With Methionine-Choline-Deficient Diet-Induced Nonalcoholic Fatty Liver Disease. J Magn Reson Imaging 2022;56:1429-36.

22. Mojtahed A, Kelly CJ, Herlihy AH, Kin S, Wilman HR, McKay A, Kelly M, Milanesi M, Neubauer S, Thomas EL, Bell JD, Banerjee R, Harisinghani M. Reference range of liver corrected T1 values in a population at low risk for fatty liver disease-a UK Biobank sub-study, with an appendix of interesting cases. Abdom Radiol (NY) 2019;44:72-84.

23. Kleiner DE, Brunt EM, Van Natta M, Behling C, Contos MJ, Cummings OW, Ferrell LD, Liu YC, Torbenson MS, Unalp-Arida A, Yeh M, McCullough AJ, Sanyal AJ; Nonalcoholic Steatohepatitis Clinical Research Network. Design and validation of a histological scoring system for nonalcoholic fatty liver disease. Hepatology 2005;41:1313-21.

24. Li J, Allen AM, Shah VH, Manduca A, Ehman RL, Yin M; NAFLD MR Imaging Research Group. Longitudinal Changes in MR Elastography-based Biomarkers in Obese Patients Treated with Bariatric Surgery. Clin Gastroenterol Hepatol 2023;21:220-222.e3.

25. Hoad CL, Palaniyappan N, Kaye P, Chernova Y, James MW, Costigan C, Austin A, Marciani L, Gowland PA, Guha IN, Francis ST, Aithal GP. A study of T1 relaxation time as a measure of liver fibrosis and the influence of confounding histological factors. NMR Biomed 2015;28:706-14.

26. Poetter-Lang S, Bastati N, Messner A, Kristic A, Herold A, Hodge JC, Ba-Ssalamah A. Quantification of liver function using gadoxetic acid-enhanced MRI. Abdom Radiol (NY) 2020;45:3532-44.

27. Fisher CD, Lickteig AJ, Augustine LM, Oude Elferink RP, Besselsen DG, Erickson RP, Cherrington NJ. Experimental non-alcoholic fatty liver disease results in decreased hepatic uptake transporter expression and

function in rats. Eur J Pharmacol 2009;613:119-27.

28. Katsube T, Okada M, Kumano S, Hori M, Imaoka I, Ishii K, Kudo M, Kitagaki H, Murakami T. Estimation of liver function using T1 mapping on Gd-EOB-DTPA-enhanced magnetic resonance imaging. Invest Radiol 2011;46:277-83.

29. Liu CY, Noda C, Ambale-Venkatesh B, Kassai Y, Bluemke D, Lima JAC. Evaluation of liver T1 using MOLLI gradient echo readout under the influence of fat. Magn Reson Imaging 2022;85:57-63.

30. Steffen IG, Weissmann T, Rothe JH, Geisel D, Chopra SS, Kahn J, Hamm B, Denecke T. Does Hepatic Steatosis Influence the Detection Rate of Metastases in the Hepatobiliary Phase of Gadoxetic Acid-Enhanced MRI? J Clin Med 2020;10:98.

31. Kirsch R, Clarkson V, Shephard EG, Marais DA, Jaffer MA, Woodburne VE, Kirsch RE, Hall Pde L. Rodent nutritional model of non-alcoholic steatohepatitis: species, strain and sex difference studies. J Gastroenterol Hepatol 2003;18:1272-82.

32. Xie Y, Zhang H, Jin C, Wang X, Wang X, Chen J, Xu Y. Gd-EOB-DTPA-enhanced T1ρ imaging vs diffusion metrics for assessment liver inflammation and early stage fibrosis of nonalcoholic steatohepatitis in rabbits. Magn Reson Imaging 2018;48:34-41.

Table S1 Effect of histopathological features on $wT1_{pre}$ according to multiple regression analyses

	B	β	t	P	F	R^2
$wT1_{pre}$					5.229**	0.170
Inflammation	−34.889	−0.506	−3.098	0.003		
Fibrosis	18.427	0.198	1.213	0.231		

**, P<0.01. $wT1_{pre}$, precontrast water-specific T1.
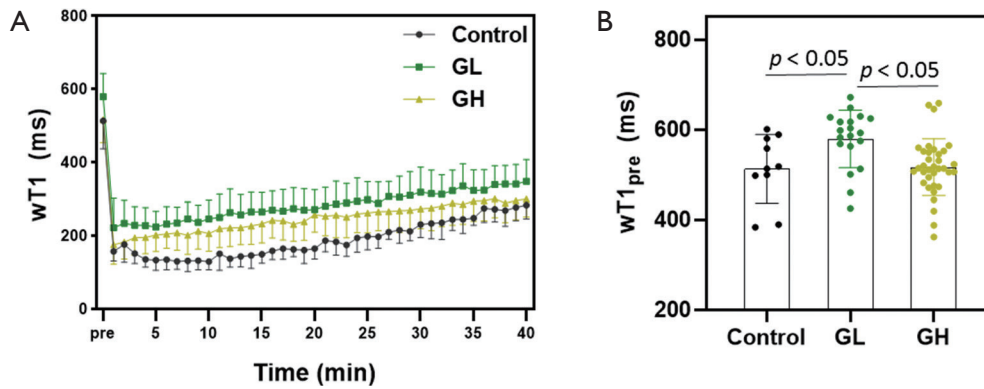
Figure S1 The dynamic wT1 change profiles across various inflammation grades. (A) The wT1 change profiles before and after Gd-EOB-DTPA administration. (B) The precontrast wT1 ($wT1_{pre}$) values across various inflammation grades. Gd-EOB-DTPA, gadolinium ethoxybenzyl-diethylenetriaminepentaacetic acid; wT1, water-specific T1; GL, none-to-mild inflammation group (G0 + G1); GH, moderate-to-severe inflammation group (G2 + G3).
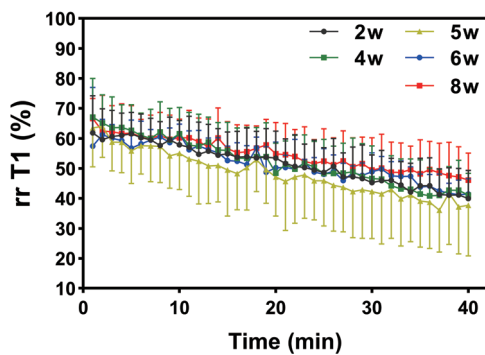

Figure S2 The rrT1 profile in the rats fed an MCD diet for 2, 4, 5, 6, and 8 weeks. Gd-rrT1, reduction rate of water-specific T1 gadolinium ethoxybenzyl-diethylenetriaminepentaacetic acid enhancement; MCD, methionine- and choline-deficient.
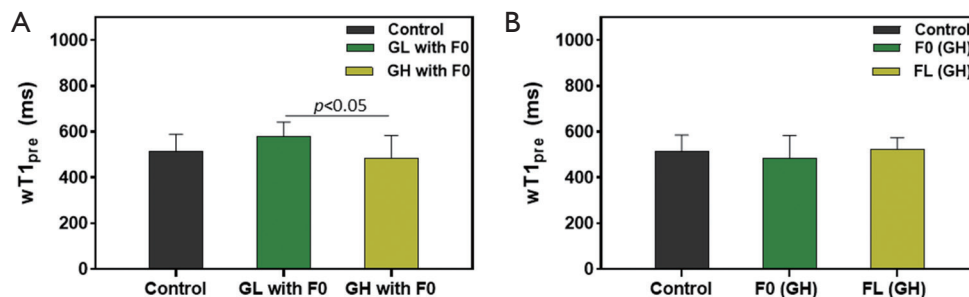

Figure S3 The $wT1_{pre}$ values in the no-fibrosis group (F0=26 rats) and the GH group (GH =35 rats). (A) The $wT1_{pre}$ values across various inflammation grades in the F0 group (control =10 rats, GL =19 rats, GH =7 rats). (B) The $wT1_{pre}$ values across various fibrosis grades in the GH group (control =10 rats, F0 =7 rats, FL =28 rats). $wT1_{pre}$, precontrast water-specific T1; GL, none-to-mild inflammation group (G0 + G1); GH, moderate-to-severe inflammation group (G2 + G3); F0, no-fibrosis group; FL, mild-to-moderate fibrosis group (F1 + F2).